JOURNAL OF APPLIED ELECTROCHEMISTRY 26 (1996) 255–267

The Li/Li^+ couple in propylene carbonate electrolytes and poly(methyl methacrylate) gels

A. M. CHRISTIE, C. A. VINCENT

Centre for Electrochemical and Material Sciences, School of Chemistry, University of St. Andrews, St. Andrews, Fife KY16 9ST, Scotland

Received 15 May 1995; revised 5 July 1995

Kinetics and mechanisms for the electrodeposition of lithium from propylene carbonate and PMMA gelled electrolytes were studied using chronoamperometric, cyclic voltammetric and chronopotentiometric methods at a nickel microelectrode. Nucleation and crystal growth models have been proposed for three salt systems. Exchange current densities, coulombic stripping efficiencies and lithium corrosion rates were evaluated.

1. Introduction

Development of a polymer electrolyte-based rechargeable lithium battery has remained a challenge since the discovery of conducting films of lithium salts in poly(ethylene oxide) in the 1970s [1, 2]. Such electrolytes have poor ambient temperature conductivities, which are generally in the range 10^{-7}–10^{-8} S cm^{-1} [3]. The gelled electrolyte alternative, consisting of a solid phase in which a conventional nonaqueous electrolyte is immobilized by a polymer matrix, offers liquid-like values for the conductivity. By varying the amount of added polymer, the viscosity of the gel may be altered to provide mechanical properties similar to that of the solid polymers, while maintaining liquid-like electrical behaviour [4–7]. High conductivity alone is not, however, sufficient for an electrolyte to be acceptable for rechargeable battery applications, and electrode/electrolyte interface and kinetic factors must also be considered.

Propylene carbonate (PC) has been used for many years as a component of liquid lithium battery electrolytes [8]. Recently, gelling agents such as poly(acrylonitrile) (PAN) and poly(methyl methacrylate) (PMMA) have been added to lithium electrolyte solutions containing PC as a main component [4–7, 9–14]. Although many electrochemical studies have been made on propylene carbonate electrolytes at conventional sized electrodes [15, 16] and microelectrodes [17, 18], very little work, other than on transport properties, has been performed on gels [13, 14]. The work presented here attempts to provide an insight into the electrochemical kinetics and mechanisms for lithium deposition at a microelectrode in such systems. Lithium hexafluorophosphate ($LiPF_6$) is compared with the salt complexes lithium bis(diglyme) hexafluorophosphate ($LiPF_6$.2DG) [19] and lithium (pentamethyldiethylene triamine) hexafluorophosphate ($LiPF_6$.PMDETA) [20, 21]. Both of these complexes have been proposed as possible alternatives for $LiPF_6$ as useful electrolytes since they have improved purity, thermal stability and conductivity in nonaqueous solution [23]. Similar studies on these systems have been performed in liquid and solid polyether media [22].

2. Experimental details

Propylene carbonate (PC) (Aldrich, 99% +) was purified using a 90 plate column Fischer HMS 500C still at 10^{-3} mbar. After refluxing for at least 1 h, the solvent was collected at a rate of approximately 25 cm^3 h^{-1}, and the middle 60% cut was kept for use and transferred to a glove box. Poly(methylmethacrylate) (PMMA) of nominal average molar mass 120 000 (99% +, Aldrich Chemical Co.) was characterized by gel permeation chromatography. The mass average was 134 000 and the number average was 67 000, giving a polydispersity index of 2. The scan showed no evidence of significant quantities of monomer or low molar mass oligomers, so that the only purification treatment for the PMMA was drying at 80 °C under vacuum for 12 h. Lithium hexafluorophosphate ($LiPF_6$) (98%, Aldrich Chemical Co. Ltd) was used as received. The complexes used in this work, kindly made available by The Associated Octel Company Ltd, were lithium-bis(diglyme)-hexafluorophosphate ($LiPF_6$.2DG) and lithium-pentamethyl-diethylene triamine-hexafluorophosphate ($LiPF_6$.PMDETA). These were synthesized using the route described in their patent [20].

Transparent gels were prepared by dissolving approximately 30 wt % PMMA in PC solutions of $LiPF_6$, $LiPF_6$.2DG and $LiPF_6$.PMDETA and casting between polished aluminium sheets heated to 90 °C. The resulting gel compositions were $LiPF_6$ (5.23)/PC (64.77)/PMMA (30.00), $LiPF_6$.2DG (13.46)/PC (56.54)/PMMA (30.00) and $LiPF_6$.PMDETA (11.42)/PC (58.58)/PMMA (30.00) by weight which were equimolal in lithium.

All experiments on the Li/Li^+ couple were carried out in two-electrode, one compartment cells. The

0021-891X

working electrode was prepared by rapidly collapsing glass onto a 25 μm diameter nickel wire, followed by cutting to reveal the microdisc. The glass seal was checked for selected samples by SEM. The electrode was polished first with alumina of decreasing sizes (1, 0.3 and 0.05 μm) suspended in water. Polishing was repeated in an argon filled dry box using 0.05 μm alumina suspended in propylene carbonate on chemically resistant polishing cloth (Beuhler), followed by rinsing with propylene carbonate. A lithium metal wire placed directly into solution was used as a counter-reference in the liquid systems and a lithium disc pressed onto a stainless steel contact was used with the solid samples. An EG&G PARC potentiostat (model 273A), controlled by an IBM compatible PC under software control (EG&G PARC electrochemical software), was used to collect the voltammetric and chronoamperometric data. Chronopotentiometry experiments were performed using a Solartron 1286 potentiostat driven by an IBM compatible PC under software control (Corrware).

To study the stability window and purity of the solvents, cyclic voltammetric studies were undertaken using a nickel microelectrode and a counter-reference electrode consisting of a lithium wire (Aldrich Chemical Co.) inserted into a glass tube containing a solution of $LiClO_4$ (1 mol dm^{-3})/propylene carbonate which was closed with a Vicor glass frit attached with heat shrinking Teflon. The experiments were undertaken with a Solartron 1286 potentiostat under software control (Corrware).

3. Results and discussion

3.1 *Solvent stabilities*

Solvents without added electrolyte may be characterised using microelectrodes. Several workers have previously studied the propylene carbonate system, suggesting that solvent reduction occurs cathodic of +1 V vs Li/Li$^+$ [24–26]. Figure 1 shows voltammograms of distilled PC at a 25 μm diameter nickel microelectrode (sweep rate = 200 mV s^{-1}). On sweeping cathodically initially (a), no cathodic process was evident and at −5 V the current density was less than 1 mA cm^{-2}. Similar results were obtained at

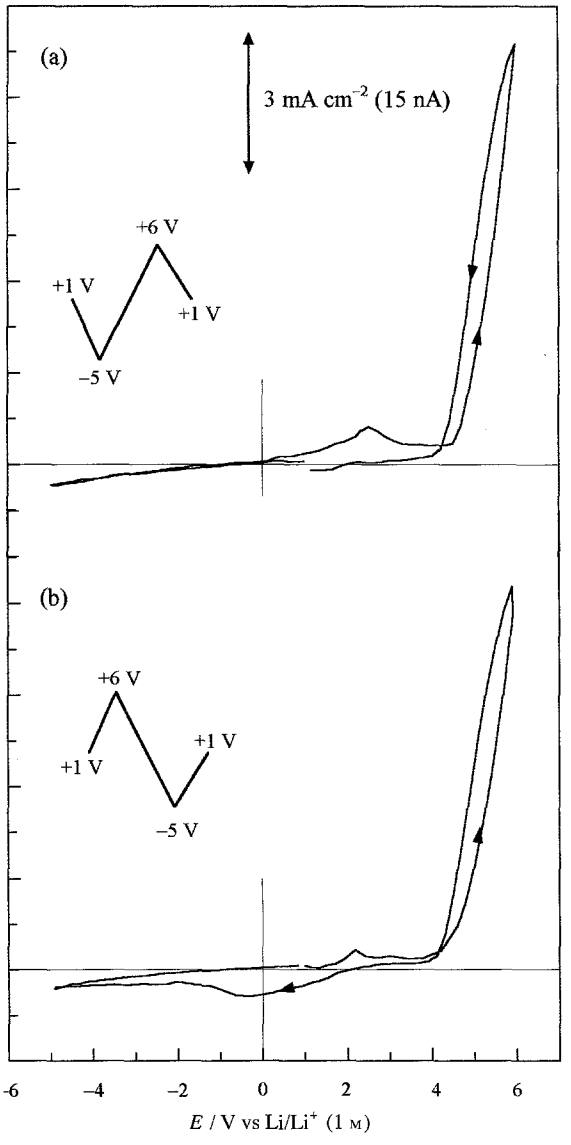

Fig. 1. Cyclic voltammograms for distilled PC at a 25 μm diameter Ni microelectrode vs Li/Li$^+$. Initial sweep direction is (a) cathodic and (b) anodic. Sweep rate: 200 mV s^{-1}.

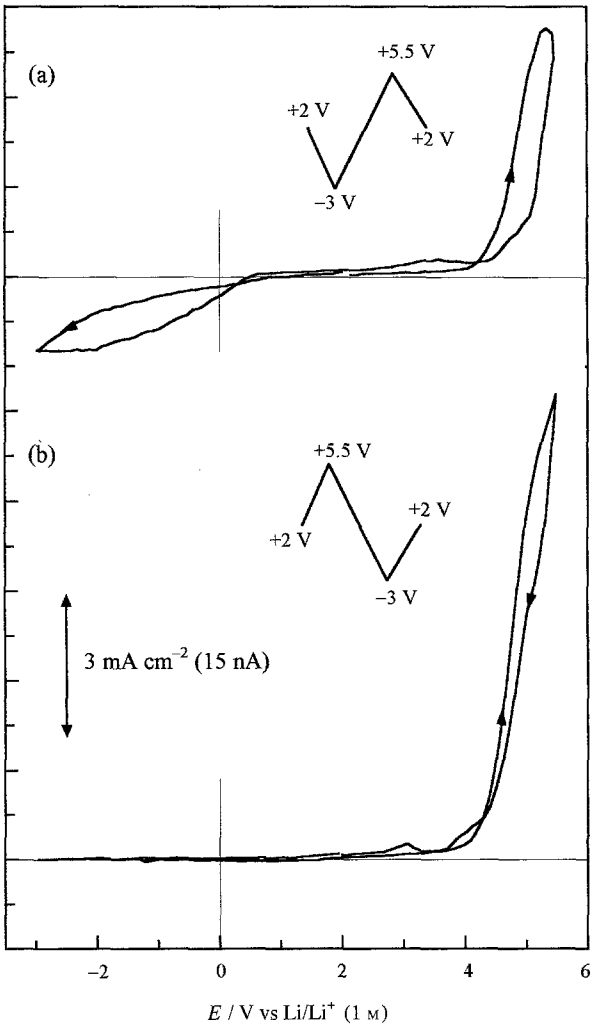

Fig. 2. Cyclic voltammograms for PC/PMMA (30 wt %) at a 25 μm diameter Ni microelectrode vs Li/Li$^+$. Initial sweep direction is (a) cathodic and (b) anodic. Sweep rate: 200 mV s^{-1}.

platinum microelectrodes (10 and 25 μm diameter). This supports the suggestion of Pletcher *et al.* [17] that the cathodic peak seen by others at approximately +1 V is attributed to reduction of trace water or some reaction product of the water with PC. Campbell *et al.* [25] have shown that a cathodic wave still exists when the water content is >15 p.p.m. It may therefore be assumed that the water content of our PC is well below the detectable range. A small anodic peak was observed commencing at +2 V due to nickel oxide formation. Anodic breakdown of PC started at +4.5 V at Ni, more than 1V lower than at Pt, agreeing well with previous literature values [17]. Sweeping anodic to +6 V initially (b), resulted in a cathodic wave in the return sweep commencing at +2 V, which did not exist when the anodic limit was lowered to +3 V. This can be attributed to the reduction of the oxidation products formed during anodic breakdown. Again, at the cathodic limit the current density was very low. Figure 2 shows voltammograms recorded for a nickel microelectrode in pure PC gelled with PMMA (30 wt %). On sweeping cathodic initially (a), a cathodic current started at approximately +1 V, possibly as a result of PMMA reduction or that of trace water as the impurity in the polymer. As in pure PC, a peak corresponding to nickel oxide formation was observed above +2 V followed by anodic breakdown of the solvent. A difference occurred on sweeping anodically first (b). The reduction wave observed in curve (a) was not seen in curve (b), suggesting that if trace water was the cause of the current then all of it was used in the formation of the passivating film and/or was involved with the electrochemical process during anodic breakdown of the solvent. The higher currents at the anodic limit of curve (b) may provide further evidence for this.

3.2. *Potentials positive of bulk lithium deposition*

On adding a lithium electrolyte a quite different I/E response was observed at potentials positive of 0 V vs Li/Li^+. Figure 3 shows three cycles of a typical voltammetric response for lithium electrolytes over a potential range of +2.5 V to 0 V at Ni. In the first cycle several peaks were observed during the cathodic sweep at (a) +1.44, (b) +1.39, (c) +0.59 and (d) +0.33 V. The anodic scan reveals two peaks at (e) +0.92 and (f) +2.07 V. Peak (a) has been shown by others [13, 17] to be due to trace water reduction, evidently introduced by the added electrolyte. Koch *et al.* [26] showed that the reduction of the AsF_6^- anion occurred at approximately +1V suggesting the possibility of the PF_6^- anion breakdown giving rise to peak (b). Peaks (c) and (d) have been attributed to the underpotential deposition (UPD) of lithium from an insoluble mixed lithium hydroxide/carbonate film present at the surface of the electrode [17, 27]. It has been shown by Aurbach *et al.* [24] that the lithium electrode surface also becomes passivated by reduction products of propylene carbonate in the presence of Li cations, and in particular by lithium alkyl carbonates. Peak (e) seems likely to correspond to the stripping of lithium from such an UPD layer, or from a lithium-nickel alloy also formed during the cathodic sweep. Reversing the sweep direction at +0.8 V, before the onset of UPD and alloy formation, results in the absence of peak (e) confirming the correlation between these two processes. Cathodic peaks in the range +0.6 to +0.3 V with a coupled anodic peak have also been observed in polyether systems [23]. Nickel oxide formation results in peak (f), as seen in the pure solvent systems. Further cycles indicate that the water content has greatly diminished with a

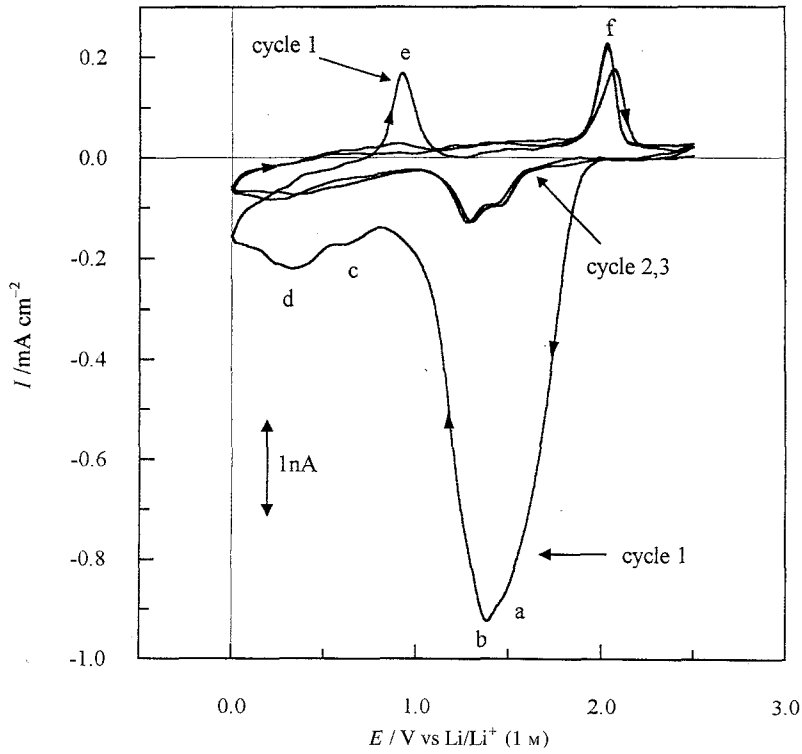

Fig. 3. Cyclic voltammogram of $LiPF_6$.PMDETA/PC/PMMA (30 wt %) at a 25 μm diameter Ni microelectrode vs Li/Li^+. Sweep rate: 10 mV s^{-1}.

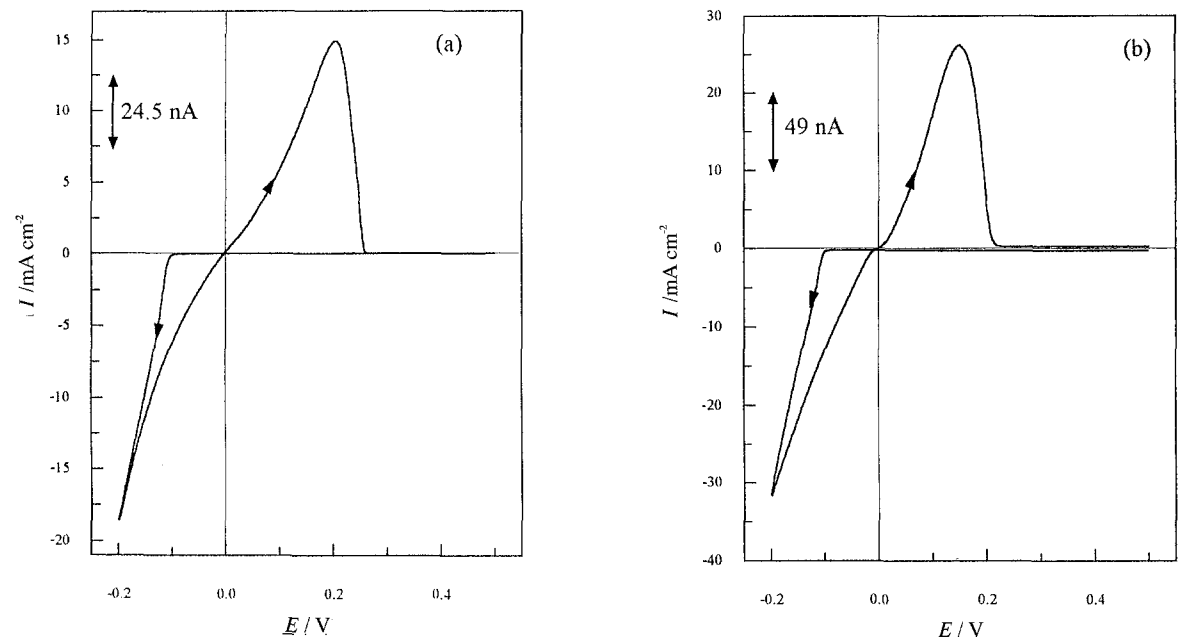

Fig. 4. Cyclic voltammogram of the lithium plating and stripping at a 25 μm diameter Ni microelectrode vs Li/Li^+ from (a) $LiPF_6$ (0.5 mol kg^{-1}) and (b) $LiPF_6$.2DG in PC. Sweep rate: 10 mV s^{-1}.

corresponding decrease in peaks (c), (d) and (e) as the quantity of lithium passivating products formed decreases. It appears that as the water content of the electrolyte increases, the amount of lithium available for UPD also increases and the corresponding voltammetry peaks become more pronounced.

3.3. *Kinetics of the Li/Li^+ couple*

Figure 4 shows voltammograms of (a) $LiPF_6$ and (b) $LiPF_6$.2DG both at 0.5 mol kg^{-1} in PC at a 25 μm diameter Ni microelectrode against Li/Li^+, recorded between +0.5 and −0.2 V at 10 mV s^{-1}. In each case the current density is very low until a sufficient overpotential has been reached for lithium nucleation to take place. The current then increases rapidly as growth of the lithium deposit occurs. This deposition process continues during the reverse scan until the equilibrium potential at 0 V has been reached, after which oxidation of the freshly deposited lithium layer

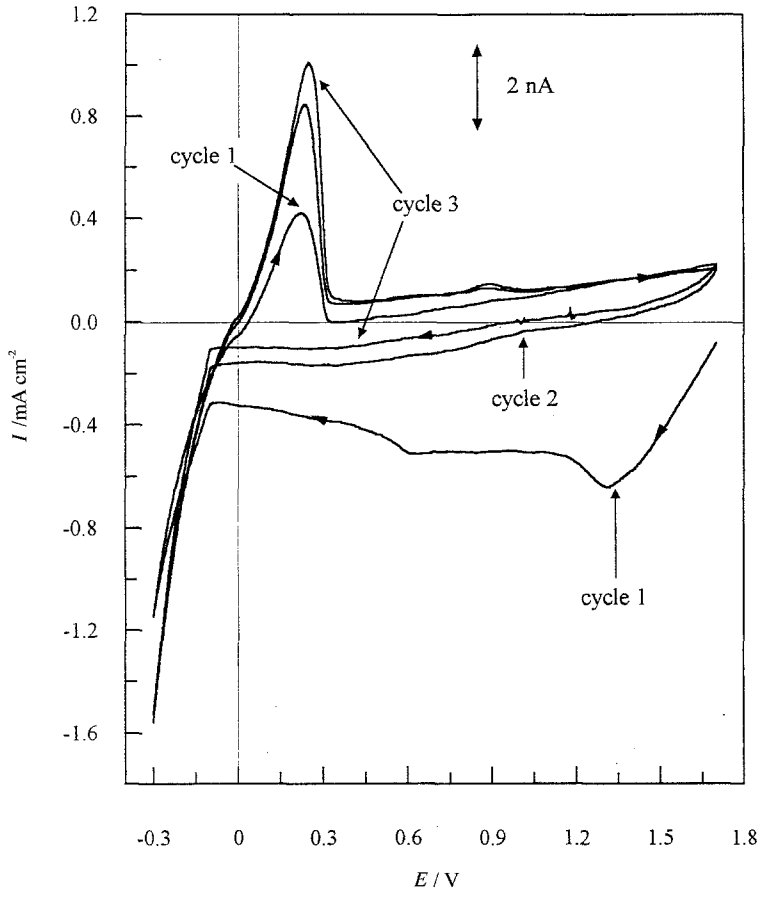

Fig. 5. Multicycle voltammogram of lithium plating and stripping from $LiPF_6$.PMDETA/PC (0.5 mol kg^{-1}) at a 25 μm diameter Ni microelectrode vs Li/Li^+.

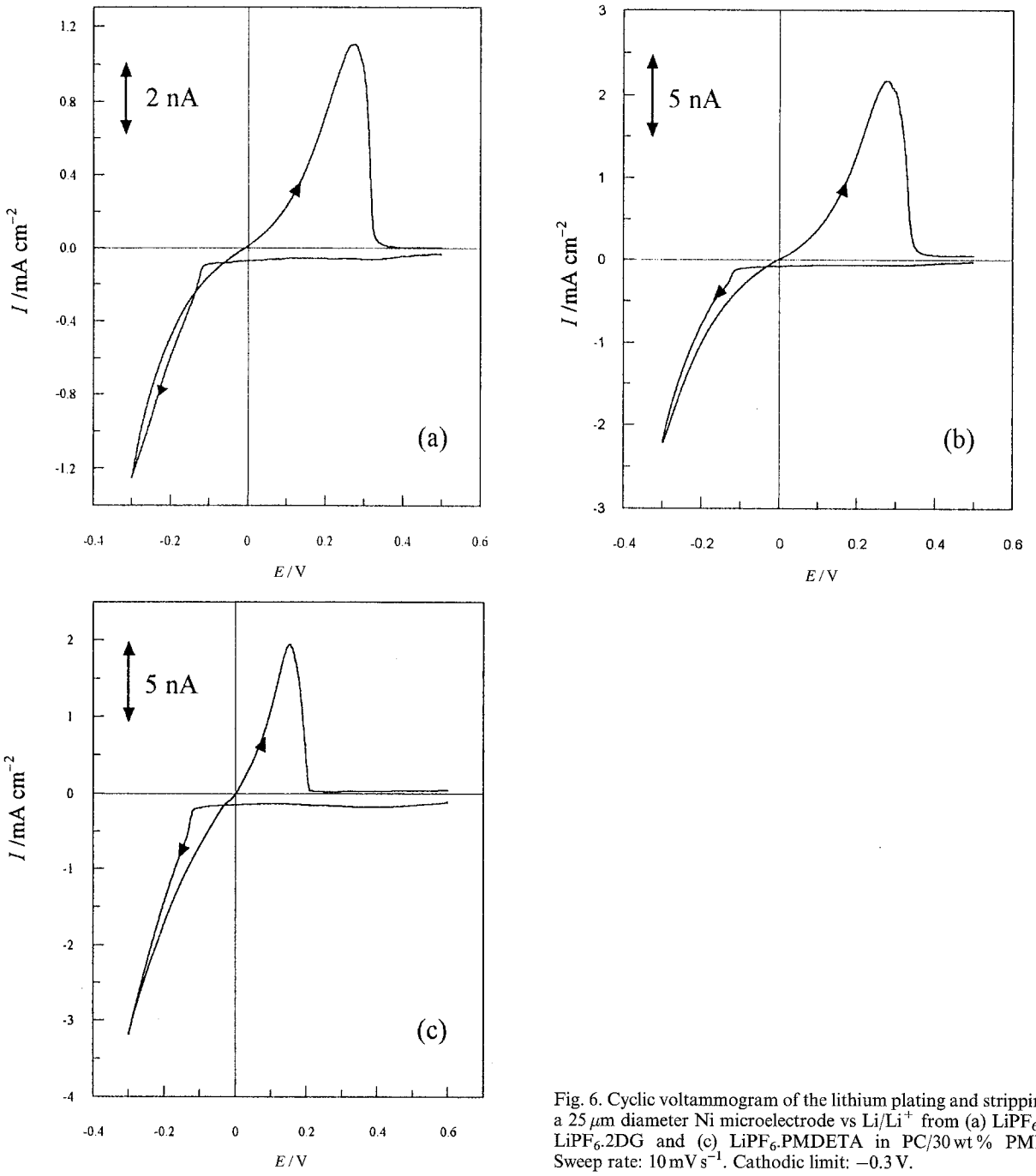

Fig. 6. Cyclic voltammogram of the lithium plating and stripping at a 25 μm diameter Ni microelectrode vs Li/Li^+ from (a) $LiPF_6$, (b) $LiPF_6$.2DG and (c) $LiPF_6$.PMDETA in PC/30 wt % PMMA. Sweep rate: 10 mV s^{-1}. Cathodic limit: −0.3 V.

proceeds with a corresponding anodic stripping peak. The current densities obtained are comparable with those obtained by Pletcher and coworkers [18] for $LiAsF_6$ in propylene carbonate. The $LiPF_6$.PMDETA complex in PC seems to produce much lower current densities, of the same order of magnitude as in solid polyethers [22]. Figure 5 shows multicycle voltammograms for $LiPF_6$.PMDETA/PC (0.5 mol kg^{-1}). The first cycle is complicated by the factors discussed above. As UPD occurred, the electrode surface became conditioned for successive cycles and the stripping efficiency increased from 29.9% in the first cycle to 97.3% in the third. Lithium plating and stripping was also performed on 30 wt % PMMA gels containing the three electrolytes. The I/E response for each system is shown in Fig. 6(a)–(c) swept between +0.5 and −0.3 V at 10 mV s^{-1}. The characteristic parameters of each electrolyte in both PC and PMMA gels are listed in Table 1. The stripping efficiencies decreased in the order $LiPF_6$ (77%) > $LiPF_6$.2DG (65%) > $LiPF_6$.PMDETA (30%) for the first cycle in propylene carbonate, while the gels decreased in the order $LiPF_6$.2DG (75%) > $LiPF_6$ (61%) > $LiPF_6$.PMDETA (26%). The values in PC are comparable with those obtained in other lithium systems [18]. On moving the cathodic limit to −0.5 V, the ratio of lithium stripped to plated increased in each case to $LiPF_6$.2DG (81%) > $LiPF_6$ (80%) > $LiPF_6$.PMDETA (40%). This would suggest that a passivating layer formed by corrosion of freshly deposited lithium is of finite thickness. As the lithium layer becomes thicker the quantity of lithium used to form this layer becomes less significant relative to the quantity deposited. The efficiencies observed with these gels are higher than those seen by Scrosati *et al.* [13] in EC:PC/PAN gels at a large nickel

Table 1. Some electrochemical parameters obtained at a 25 μm Ni microelectrode vs Li/Li^+ by cyclic voltammetry
Sweep rate $\nu = 10\,mV\,s^{-1}$, $T = 298\,K$.

Electrolyte		*Nucleation overpotential*	*Cathodic current density at*	*Exchange current density*	*Transfer coefficients*	*Peak potentials*	*Stripping efficiency*
Solvent	*Salt*	η/mV	$\eta = 200\,mV$ I/mA cm^{-2}	I_0/mA cm^{-2}	$(n\alpha)_A$	E_P^A/mV	*(1st cycle)*
PC	$LiPF_6$ (0.5 mol kg^{-1})	103	18.5	1.06^{BV} 1.21^{L}	0.48	203	77.0
	$LiPF_6$.2DG (0.5 mol kg^{-1})	103	31.5	2.34^{BV} 0.901^{L}	0.53	151	65.0
	$LiPF_6$.PMDETA (0.5 mol kg^{-1})	91.0	0.654	0.042^{BV} 0.041^{L}	0.45	224	29.9
PC/PMMA 30 wt %	$LiPF_6$ (0.5 mol kg^{-1} PC)	107	0.593	0.0290^{BV} 0.0377^{L}	0.53	274	60.6
	$LiPF_6$.2DG (0.5 mol kg^{-1} PC)	115	0.782	0.0579^{BV} 0.0622^{L}	0.50	274	75.3
	$LiPF_6$.PMDETA (0.5 mol kg^{-1} PC)	120	1.43	0.150^{BV} 0.138^{L}	0.59	155	26.4

BV = Values calculated from a NLLS fit to Butler–Volmer curve.
L = Linear part of CV at low overpotentials.

electrode. Nucleation overpotentials decrease in the order $LiPF_6$, $LiPF_6$.2DG > $LiPF_6$.PMDETA in PC and $LiPF_6$.PMDETA > $LiPF_6$.2DG > $LiPF_6$ in the PMMA gels. This reversal of order from PC to gel suggests that the polymer interacts with the cation and more significantly with the complexed cation. However, once the appropriate overpotential has been reached, the rate of deposition was more rapid for each of the complexes than for the simple salt. Exchange current densities were calculated from non-linear least squares (NLLS) fitting of the reverse sweep of the voltammograms to the Butler-Volmer equation. Figure 7 shows typical NLLS fits to (a) the reverse sweep and (b) the Tafel slopes of the voltammogram for $LiPF_6$/PC/PMMA. The exchange current densities determined in this way were compared with those obtained from a linear approximation to the Butler–Volmer equation at very low overpotentials, defined previously [22].

The kinetics of the Li/Li^+ couple were studied further by performing a series of potential-step experiments. A cathodic potential step was applied (−150 mV: $LiPF_6$/PC, −150 mV: $LiPF_6$.2DG/PC, −300 mV: $LiPF_6$.PMDETA/PC/PMMA, −300mV: $LiPF_6$/PC/PMMA, −250 mV: $LiPF_6$.2DG/PC/PMMA and −250 mV: $LiPF_6$.PMDETA/PC/PMMA), passing approximately 0.5 C cm^{-2} of charge, to deposit a layer of lithium. The potential was then stepped to an anodic potential in the range +75 to +300 mV. A set of transients for the anodic polarization of a freshly deposited lithium layer from $LiPF_6$/PC is shown in Fig. 8. After application of the anodic step the lithium oxidizes at an approximately uniform rate until the layer is depleted. Reactivation, or pitting, of the deposit at higher overpotentials results in the current transient passing through a peak. By varying the cathodic deposition potential over the range −75 to −400 mV and applying for 5 s, the current

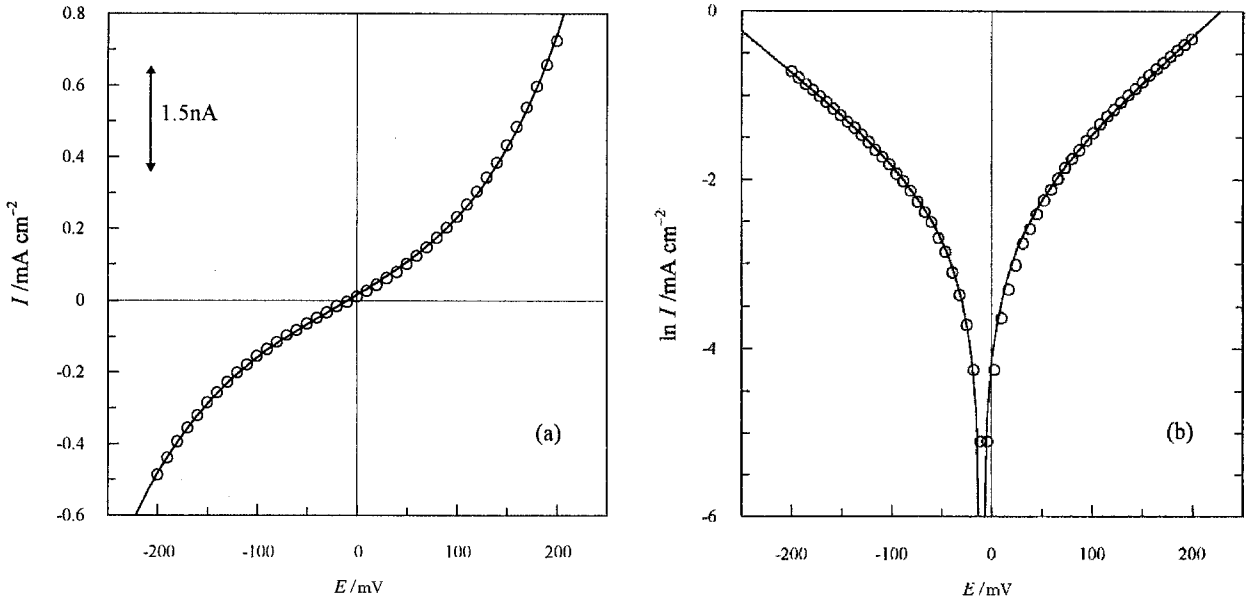

Fig. 7. (a) Reverse sweep and (b) Tafel slopes of the voltammogram for $LiPF_6$/PC/PMMA at 10 mV s^{-1}. The solid lines represent the NLLS fit to the Butler–Volmer equation.

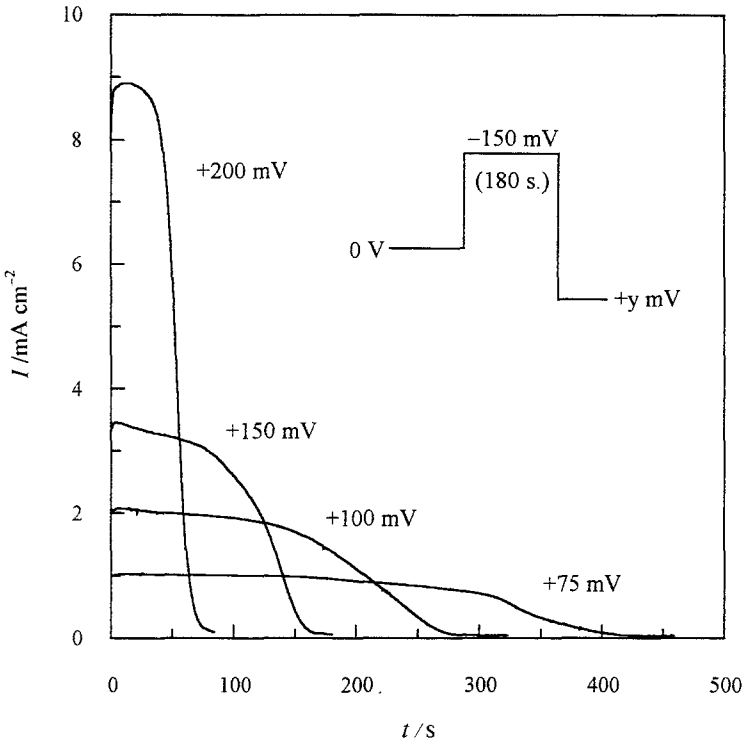

Fig. 8. Anodic polarization of deposited lithium from $LiPF_6$/PC at a 25 μm diameter microelectrode vs Li/Li^+ after deposition of 0.5 C cm^{-2} charge at −150 mV.

transients reach steady state plateaux corresponding to thickening of the lithium layer. The steady-state current plateau from each of the polarization curves can be used to construct a Tafel plot. The Tafel plots for the PC solutions and PMMA gels are shown Fig. 9(a) and (b), respectively. Straight lines are observed in each case corresponding to charge-transfer control. Deviations from the Tafel slopes at very low overpotentials indicate the lower limit to which the limiting form of the Butler–Volmer expression can be used. The currents deviate from the Tafel line at high overpotentials where mass transport control dominates. The transfer coefficients and exchange current densities were determined from the slopes and intercept of the lines extrapolated to the equilibrium potential. Table 2 lists the results of this analysis. Taking into consideration the different method for lithium deposition, the values obtained compare well with those determined from the cyclic voltammetric experiments.

3.4. *Nucleation and growth of the lithium deposit*

Any electrochemical phase transformation generally involves either two or three-dimensional nucleation processes during the early stages [28, 29]. The number of nuclei and rate of formation is strongly dependent on the overpotential applied. Chronoamperometry involves the application of a potential-step while recording the current transient, analysis of which can provide an insight into the morphology of the deposit growing at the electrode surface. Figure 10

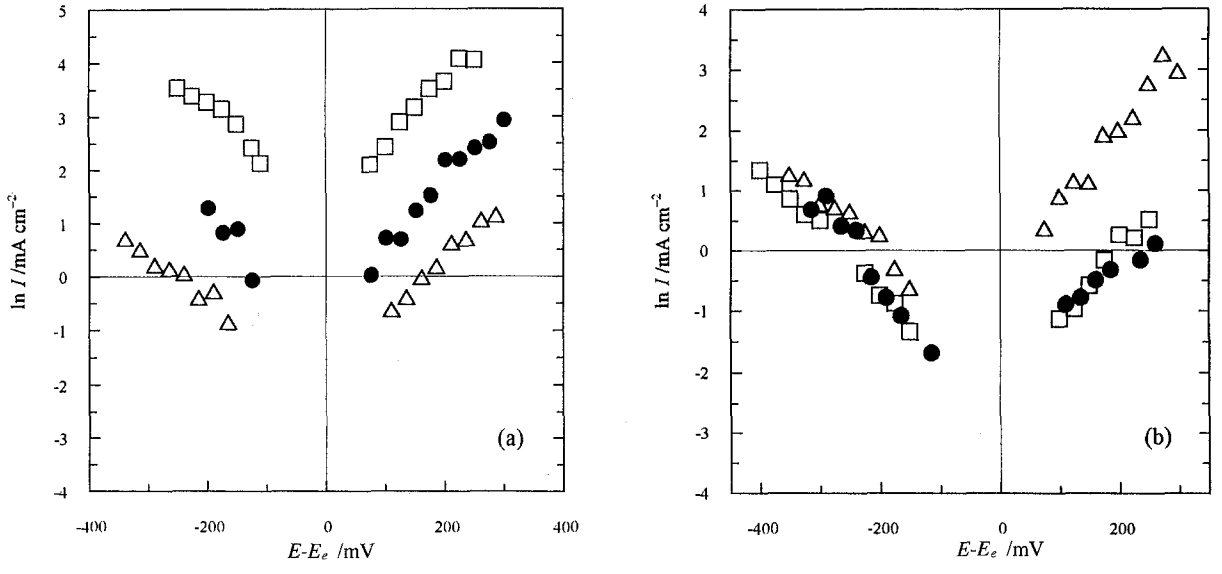

Fig. 9. Tafel slopes obtained from steady-state current transients of freshly deposited lithium at a 25 μm diameter Ni microelectrode vs Li/Li^+. Data points represent (●) $LiPF_6$, (□) $LiPF_6$.2DG and (△) $LiPF_6$.PMDETA each in (a) PC and (b) PC/30 wt % PMMA.

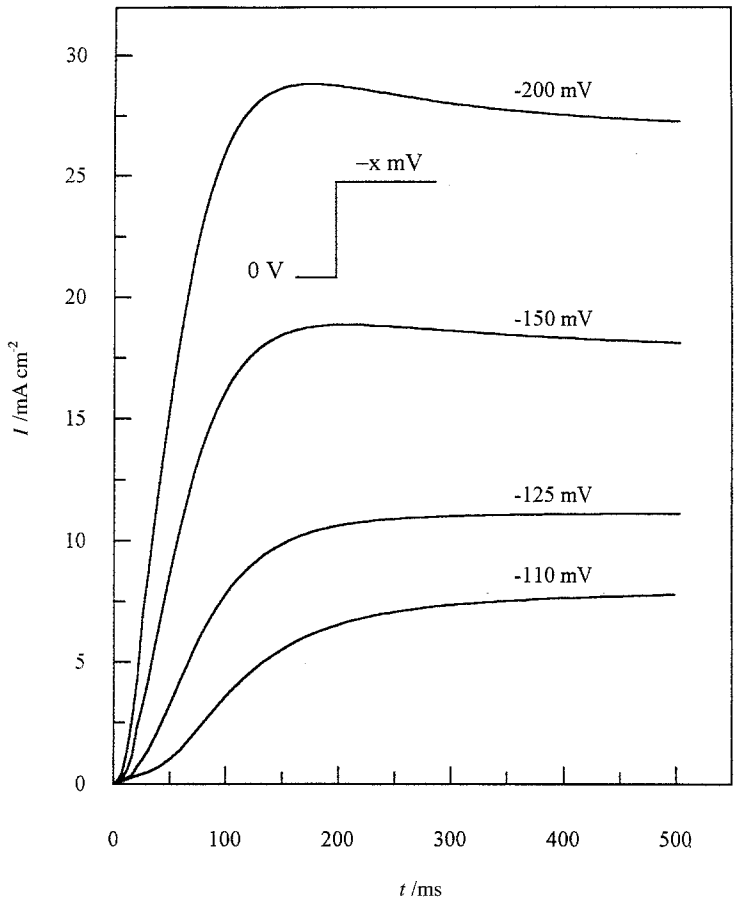

Fig. 10. Current transients for the nucleation and growth of lithium from $LiPF_6$.2DG/PC (0.5 mol kg^{-1}) at a 25 μm diameter microelectrode vs Li/Li^+. The overpotentials applied are indicated in the Figure.

shows a set of experimental current transients for propylene carbonate containing $LiPF_6$.2DG (0.5 mol kg^{-1}). As the electroactive area of the deposit grows, the current rises and approaches a steady state value where continuous thickening of the layer takes place. On increasing the value of the potential step the lithium is deposited at a higher rate and the rise time to the steady-state plateau decreases. The general appearance of the I/t transients have the features of a three-dimensional nucleation and growth process. At longer time scales the current rises once more indicating a further increase in the surface area, likely to be due to growth of the deposit over the glass surrounds of the microelectrode [30]. At potential-steps lower than the nucleation overpotentials listed in Table 1 rising transients were not observed on the experimental time-scale.

The initial rising transient follows a function of t^n, where n depends on the type of nucleation, the geometry of the nuclei and the rate determining step of nuclei incorporation into a growing cluster. It has been shown previously [22, 23] that nonlinear least-squares fits to prolonged current-transient expressions were preferable in comparison with a simple linear fit of the rising section to the appropriate function of t. The equations describing three-dimensional nucleation can be simplified, as shown before [22], to

$$I = a\{1 - \exp(bt^2)\} \quad (1)$$

$$I = a\{1 - \exp(ct^3)\} \quad (2)$$

for kinetic controlled growth of cones or hemispheres following three-dimensional instantaneous and progressive nucleation, respectively, where I is the current density and t is the time; and

$$I = \frac{d}{\sqrt{t}}\{1 - \exp(et)\} \quad (3)$$

$$I = \frac{d}{\sqrt{t}}\{1 - \exp(ft^2)\} \quad (4)$$

for diffusion controlled growth of hemispheres following three dimensional instantaneous and progressive nucleation, respectively. The parameters a–f are arbitrary variables calculated during each fit.

Figure 11 shows the NLLS fit at each potential as solid lines, clearly indicating the close correlation between the experimental data and the model for instantaneous nucleation followed by kinetic controlled growth of cones or hemispheres. A clear difference between the instantaneous and progressive nucleation models can be observed, where a simulation

Table 2. The exchange current densities and transfer coefficients for PC and PMMA gelled electrolytes, obtained from Tafel plots

Electrolyte		I_0 /mA cm^{-2}	$(n\alpha)_C$	$(n\alpha)_A$
Solvent	*Salt*			
PC	$LiPF_6$	1.08	0.14	0.24
	$LiPF_6$.2DG	2.82	0.29	0.36
	$LiPF_6$.PMDETA	0.146	0.19	0.29
PC/PMMA	$LiPF_6$	0.134	0.22	0.24
	$LiPF_6$.2DG	0.0700	0.26	0.37
	$LiPF_6$.PMDETA	0.483	0.13	0.39

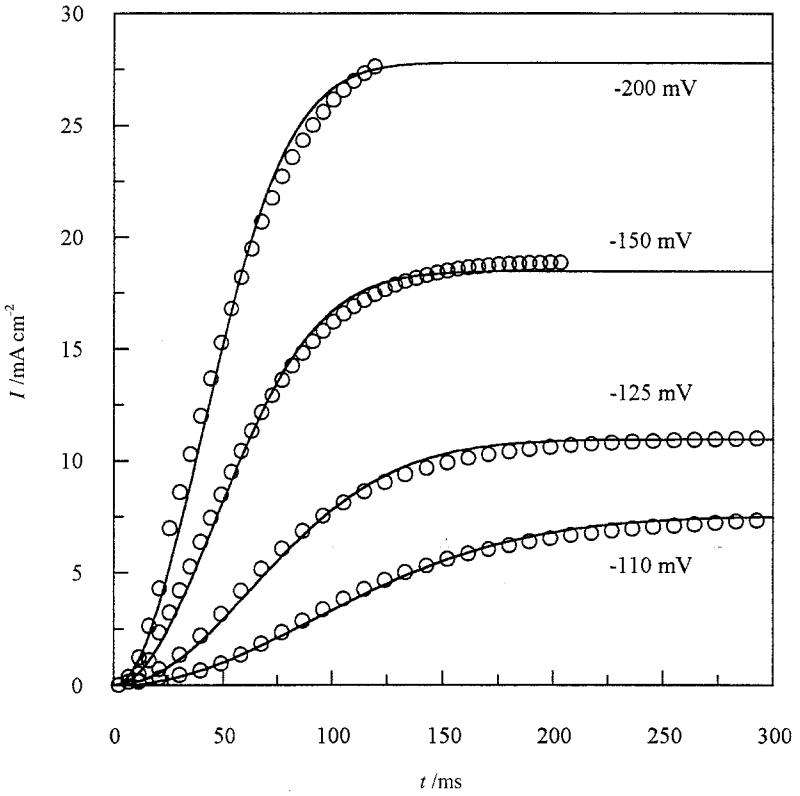

Fig. 11. Current transients at various overpotentials for $LiPF_6$.2DG/PC at a 25 μm diameter microelectrode vs Li/Li^+. The solid lines indicate NLLS fits for instantaneous nucleation followed by kinetic controlled growth of cones or hemispheres.

of progressive nucleation does not follow the experimental transient. The decay time of the charging currents in the gel electrolyte systems were comparatively long, resulting in distortion of the I/t curves during the early stages. This resulted in a difficult analysis which relied on well formed transients after the decay of the charging current. A typical curve is shown in Fig. 12 for the deposition of lithium from $LiPF_6$.2DG/PC/PMMA with the corresponding NLLS fit. All the electrolytes, in both PC and PC/PMMA gels, appear to undergo instantaneous three-dimensional nucleation followed by kinetic controlled growth. In some cases, at very high overpotentials, the transients pass through a small peak before reaching their steady-state values. This is most likely due to a contribution of linear diffusion, similar to that seen at a conventional sized electrode, since a pure hemispherical diffusion zone does not exist on the time-scale of the experiments at a 12.5 μm radius microdisc.

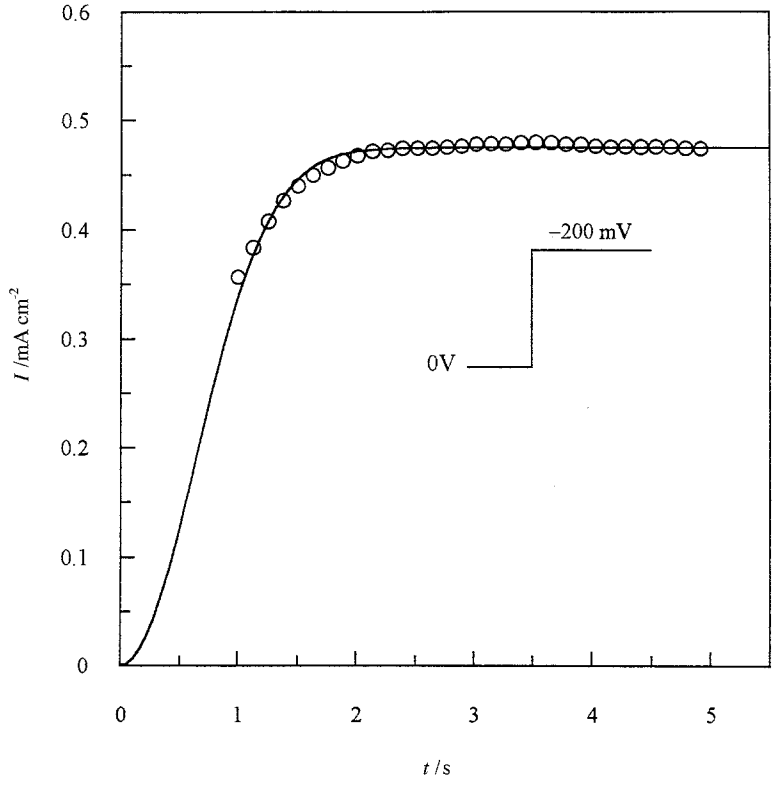

Fig. 12. Current transient at −200 mV for $LiPF_6$.2DG/PC/PMMA at a 25 μm diameter microelectrode vs Li/Li^+. The solid lines indicate the NLLS fit for instantaneous nucleation followed by kinetic controlled growth of cones or hemispheres.

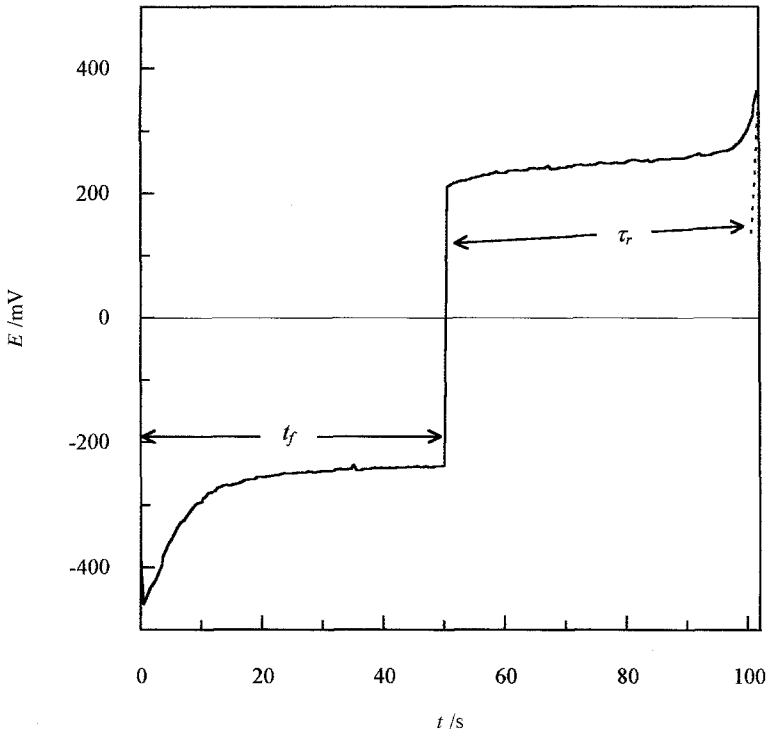

Fig. 13. Current reversal chronopotentiogram for $LiPF_6$.2DG/PC/PMMA at a 25 μm diameter microelectrode. $i_f = i_r = 4$ nA (0.81 mA cm^{-2}).

3.5. *Lithium reactivity and passivation*

A typical current reversal chronopotentiogram is shown in Fig. 13 obtained from $LiPF_6$.2DG/PC/PMMA at a Ni microelectrode, where the applied cathodic (forward) and anodic (reverse) currents were both 4 nA (0.81 mA cm^{-2}). Current reversal chronopotentiometry (CRC) involves the application of a galvanostatic cathodic pulse for a time t_f to deposit a layer of lithium at the nickel surface before reversing the pulse. On application of the anodic pulse the lithium is uniformly stripped until the surface concentration becomes zero, and the potential moves rapidly positive until reaching another anodic process. The time taken to reach completion of lithium oxidation is termed the reverse transition time τ_r. The ratio τ_r/t_f provides a useful means of determining galvanostatic stripping efficiencies, and any departure of this ratio from unity indicates a following chemical reaction of the lithium [31, 32], assuming there is no significant diffusion away from the electrode surface.

The effect of electrode passivation may be established by applying a series of CRCs without repolishing the electrode between cycles. Figure 14 shows (a) a multicycling E/t transient for $LiPF_6$/PC, and (b) a plot of the calculated current efficiencies against cycle number for the propylene carbonate solutions. In each case the efficiency increases after the first cycle, suggesting that a significant quantity of lithium is used to condition the nickel surface via anodic film and lithium–nickel alloy formation. Successive cycles for $LiPF_6$ show that after reaching a stripping efficiency of approximately 76%, the quantity stripped begins to decrease steadily after the 4th cycle to 63% in the 9th, indicating passivation or loss of lithium. The $LiPF_6$.PMDETA efficiency increases rapidly to over 78% in the 4th cycle, remaining approximately constant thereafter. After increasing to 58% after the 1st cycle, the efficiency of stripping from $LiPF_6$.2DG decreased to a steady value of approximately 55% after cycle 5. When gelled, the performances of $LiPF_6$ and $LiPF_6$.2DG improved significantly to above 90% stripping efficiency, while the $LiPF_6$.PMDETA complex remained below 70%. The corrosion current I_{corr} was determined as before [22] using

$$I_{corr} = I_{appl}\left(\frac{t_f - \tau_r}{t_f + \tau_r}\right) = I_{appl}\left(\frac{1 - \tau_r/t_f}{1 + \tau_r/t_f}\right) \quad (5)$$

where I_{appl} is the applied current density. When the ratio τ_r/t_f remains constant at different t_f, the rate of lithium corrosion (in mol cm^{-2} s^{-1}) is given by

$$k_l = \frac{I_{corr}}{F} \quad (6)$$

Table 3 shows the calculated values of the rate of lithium loss k_l. In general, the rate of lithium loss was significantly lower with the gels than with the liquid PC.

It has been generally accepted that lithium is

Table 3. Rate of lithium corrosion, k_l, obtained from CRC

Electrolyte		*Rate of lithium loss, k_l* /mol s^{-1} cm^{-2}	I_{appl} /mA cm^{-2}
Solvent	*Salt*		
PC	$LiPF_6$	1.06×10^{-9}	0.81
	$LiPF_6$.2DG	2.21×10^{-9}	0.81
	$LiPF_6$.PMDETA	9.93×10^{-10}	0.81
PC/PMMA	$LiPF_6$	3.50×10^{-10}	0.81
	$LiPF_6$.2DG	4.35×10^{-10}	0.81
	$LiPF_6$.PMDETA	1.73×10^{-9}	0.81

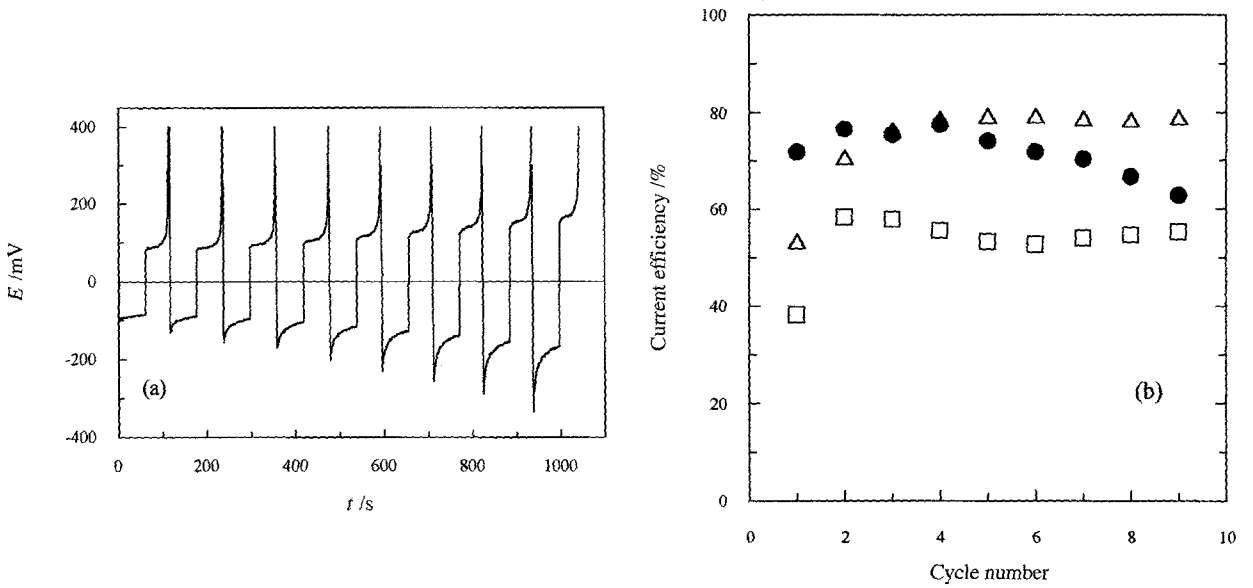

Fig. 14. (a) multicycling chronopotentiogram for $LiPF_6$/PC at a Ni microelectrode. (b) Current efficiencies vs cycle number for PC containing (●) $LiPF_6$, (□) $LiPF_6$.2DG and (△) $LiPF_6$.PMDETA. $t_f = 60$ s, $i_f = i_r = 4$ nA (0.81 mA cm^{-2}).

unstable in the presence of propylene carbonate solutions, forming insoluble films at the surface of the lithium, the composition of which can be electrolyte dependent [33, 34]. This passivation behaviour of the freshly deposited lithium was investigated by the measurement of the coulombic stripping efficiencies following periods on open-circuit. A double potential-step was applied in each case to deposit a lithium layer (charge passed was approximately 0.5 C cm^{-2}). A controlled delay between the cathodic and anodic pulses allowed the cell to rest at open-circuit before stripping the lithium off the electrode at +150 mV in each case. Figure 15 shows a plot of the coulombic stripping efficiencies against time on open-circuit for all prepared electrolytes. The efficiencies of $LiPF_6$/PC and $LiPF_6$.PMDETA/PC remained steady at

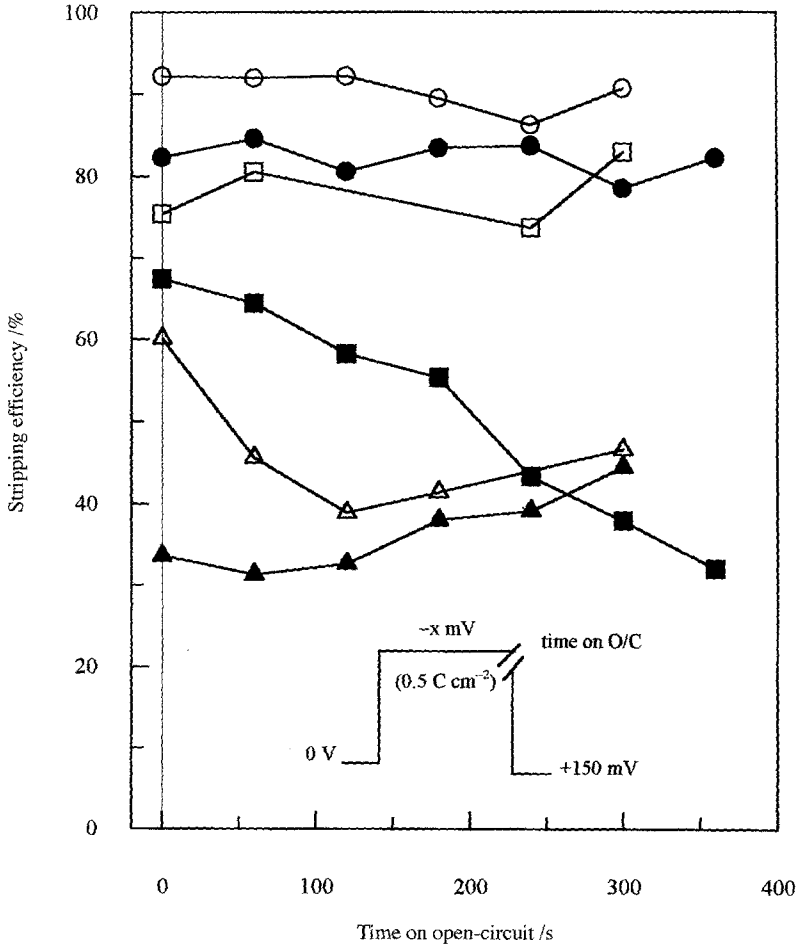

Fig. 15. Plot of coulombic stripping efficiency vs time on open circuit of freshly deposited lithium from (●) $LiPF_6$/PC, (■) $LiPF_6$.2DG/PC, (▲) $LiPF_6$.PMDETA/PC/PMMA, (○) $LiPF_6$/PC/PMMA, (□) $LiPF_6$.2DG/PC/PMMA and (△) $LiPF_6$.PMDETA/PC/PMMA.

approximately 80% and 35–40%, respectively, indicating that any surface films were formed rapidly. The profile of the $LiPF_6$.2DG/PC plot, however, indicates continuing reaction of the deposited lithium using the majority of the available deposit suggesting that the film was either soluble in the solvent medium or extremely thick. The passivating nature in the $LiPF_6$/PC/PMMA gel was found to be similar to that in PC, but here the stripping efficiency increased to approximately 92%. The diglyme complex appeared to be more stable in the gel, with stripping efficiencies around 80% and stable over a longer period. This highlights the considerable differences between the passivating films formed. Although the efficiency of the PMDETA complex in the PC/PMMA gel was initially approximately 60%, growth of the passivating film reduces this value to about 40%, similar to its performance in PC. This may be simply showing the difference in the rates of growth of essentially similar films.

4. Conclusions

Although trace impurities such as water will be a common feature in the manufacture of real battery electrolytes, it is important to identify the role played by such contaminants. Evidence given here for the cathodic stability of pure propylene carbonate at a nickel microelectrode, without added electrolyte, confirms the suspicions of Pletcher [17] that the cathodic wave or peak observed by others [24–26] is more than likely due to the presence of water and/or oxygen. Cyclic voltammetric studies at potentials anodic of bulk lithium deposition revealed several peaks thought to be due to the underpotential deposition of lithium by reduction of lithium ions in the passivating layer.

The cyclic voltammetry and potential-step experiments show the kinetics of the Li/Li^+ couple to be fast in both propylene carbonate and propylene carbonate gelled with poly(methyl methacrylate). The ligands evidently play an important role by increasing the currents observed in both PC and the gels. Results from cyclic voltammetry clearly show that a crystallization process occurs in each case at the nickel microelectrode surface with varying deposition rates, resulting in different stripping efficiencies, all well below 80%. Chronoamperometry measurements showed that all the systems essentially follow the same three-dimensional nucleation and growth models, although the gels not surprisingly suffer from long decay times of the charging currents during the early stages of the transient. Galvanostatic and double potential-step experiments indicate that the $LiPF_6$/PC/(30 wt %) PMMA and $LiPF_6$.2DG/PC/(30 wt %) PMMA gels have high stripping efficiencies above 90%. The high viscosity of these gels may be sufficient to hinder dendritic growth, normally present in the liquid cell where growth of the deposit has more freedom, thus making more lithium available for electrochemical oxidation. The differences between the stripping efficiencies obtained by cyclic voltammetry, chronopotentiometry and potential-step experiments may be attributed to the morphology of the deposit caused by variations in deposition rate. In cases where stripping was inefficient, the deposit may consist largely of dendrites or needles which are unavailable for anodic dissolution.

Acknowledgements

Thanks are given to The Associated Octel Company Ltd and the Engineering and Physical Sciences Research Council for financial Support.

References

[1] P.V. Wright, *Br. Polymer J.* **7** (1975) 319.
[2] M.B. Armand, J.M. Chabagno and M. Duclot, 2nd International Meeting on Solid Electrolytes, St. Andrews, Scotland (1978).
[3] M. Armand, *Solid State Ionics* **9/10** (1983) 745.
[4] K.M. Abraham and M. Alomgir, *J. Power Sources* **43/44** (1993) 195–208.
[5] O. Bohnke, G. Frand, M. Rezrazi, C. Rousselot and C. Truche, *Solid State Ionics* **66** (1993) 97–104.
[6] O. Bohnke, G. Frand, M. Rezrazi, C. Rousselot and C. Truche, *ibid.* **66** (1993) 105–12.
[7] M. Ue, M. Kaitoh, E. Yasukawa and S. Mori, *Electrochim Acta* **38** (1993) 1301.
[8] J. P. Gabano (Ed.), 'Lithium Batteries', Academic Press, London (1983).
[9] H. Huang, L. Chen, X. Huang, R. Xue, C. Liquor, H. Xuejie and X. Rangjian, *Electrochim. Acta* **37** (1992) 1671–73.
[10] R. Xue, H. Huang, L. Chen and K. Wang, *Solid State Ionics* **59** (1993) 1–4.
[11] F. Croce, S.D. Brown, S.G. Greenbaum, S. Slone and M. Soloman, *Chem. Mater.* **5** (1993) 1268–72.
[12] R. Xue, H. Huang, M. Menetier and L. Chen, *J. Power Sources* **43/44** (1993) 431–38.
[13] G. Dautzenberg, F. Croce, S. Passerini and B. Scrosati, *Chem. Mater.* **6** (1994) 538–42.
[14] G. Nagasubramanian, A.I. Attia and G. Halpert, *J. Appl. Electrochem.* **24** (1994) 298–302.
[15] R.D. Rauh and S.B. Brummer, *Electrochim. Acta* **22** (1977) 75.
[16] G. Nazri and R.H. Muller, *J. Electrochem. Soc.* **132** (1985) 2054.
[17] D. Pletcher, J.F. Rohan and A.G. Ritchie, *Electrochim. Acta* **39** (1994) 1369.
[18] D. Pletcher, J.F. Rohan and A.G. Ritchie, *ibid.* **39** (1994) 2015.
[19] Duracell Inc., 'Improved method for preparing non-aqueous electrolytes', *European Patent appl. 90 302 078.2* (Sept. 1990).
[20] The Associated Octel Company Ltd., 'Lewis base complexes of alkali metal salts,' *European patent appl. 88 309 912.7* (Oct. 1988).
[21] D.S. Wright, PhD thesis, Cambridge, England (1989).
[22] A.M. Christie, A. Lisowska-Oleksiak and C.A. Vincent, *Electrochim. Acta*, **40** (1995) 2405.
[23] A.M. Christie, PhD thesis, St. Andrews, Scotland (1995).
[24] D. Aurbach and H. Gottlieb, *Electrochim. Acta* **34** (1989) 141.
[25] S.A. Campbell, C. Bowes and R.S. McMillan, *J. Electroanal. Chem.* **284** (1990) 195.
[26] C. Nanyundiah, J.L. Goldman, L.A. Dominey and V.R. Koch, *J. Electrochem. Soc.* **135** (1988) 2914.
[27] D. Wagner and H. Gerischer, *Electrochim. Acta* **34** (1989) 1351.
[28] G. Gunuwardena, G. Hills, I. Montenegro and B. Scharifker, *J. Electroanal. Chem.* **159** (1983) 264.
[29] M. Fleischmann and H.R. Thirsk, *in* 'Advances in Electrochemistry and Chemical Engineering', Vol. 3 (edited by

P. Delahay and C.W. Tobias), Interscience, New York (1962) p. 123.
[30] J.D. Genders, W.M. Hedges and D. Pletcher, *J. Chem. Soc. Faraday Trans. I* **80** (1984) 3399.
[31] T. Berzins and P. Delahay, *J. Amer. Chem. Soc.* **75** (1953) 4205.
[32] R.K. Jain, H.C. Gaur and B.J. Welch, *J. Electroanal. Chem.* **79** (1977) 211.
[33] D. Aurbach, M.L. Daroux, P.W. Faguy and E. Yeager, *J. Electrochem. Soc.* **134** (1987) 1611.
[34] D. Aurbach, Y. Ein-Ely and A. Zaban, *ibid.* **141** (1994) L1–L3.